

Role of elasticity associated with oxygen ordering in $\text{YBa}_2\text{Cu}_3\text{O}_z$

M. Goldman and C. P. Burmester

*Department of Materials Science & Mineral Engineering, and Materials Sciences Division, Lawrence Berkeley Laboratory,
University of California, Berkeley, California 94720*

L. T. Wille

Department of Physics, Florida Atlantic University, Boca Raton, Florida 33431

R. Gronsky

*Department of Materials Science & Mineral Engineering, and Materials Sciences Division, Lawrence Berkeley Laboratory,
University of California, Berkeley, California 94720*

(Received 27 February 1995; revised manuscript received 22 March 1995)

A Monte Carlo technique incorporating elasticity is applied to simulate oxygen-vacancy ordering and concomitant elastic distortion within the basal plane of $\text{YBa}_2\text{Cu}_3\text{O}_z$. The simulation model employs an extension of an anisotropic Ising model to account for small displacements of copper, oxygen, and vacancy positions within the basal plane so that the simultaneous evolution of atomic positions and occupancies can be examined. Simulations performed with this model are first compared to previous studies of oxygen-vacancy ordering under a static lattice approximation, and then used to investigate the contribution of elastic strain to the formation of experimentally observed $\sqrt{2}$ superstructures, deformation twinned, twinning, nucleation and growth of ordered domains, and the nature of the tetragonal-to-orthorhombic transition occurring in this system. The influence of elasticity on microstructural evolution is examined via simulations of rapid quenching through the tetragonal-to-orthorhombic transition or of deformation of the orthorhombic phase to induce strain, both followed by annealing. Results are presented as lattice configuration photographs, fast Fourier transform intensity distributions, and strain maps. The formation and evolution of these microstructures are rationalized in terms of the accommodation of strain energy accumulated during the course of the simulated thermomechanical treatments. The formation of the $\sqrt{2}a_0 \times \sqrt{2}a_0$ structure is found to result from strain dissipation via a softened phonon mode with wave vector $\mathbf{q} = [\frac{1}{2} \frac{1}{2} 0]$.

I. INTRODUCTION

In the last decade enormous progress has been made towards a theoretical description of phase transformations in metallic alloys based upon "first-principles" quantum mechanics.¹ Phase diagrams for a wide variety of substitutional binary alloys can now be readily calculated, while ternary and even quaternary systems are not far behind. Typically, these computations start with an *ab initio* electronic band-structure calculation to find effective pair interactions (EPI's) describing the ordering energies, followed by classical statistical mechanics to calculate a phase diagram. The assumptions and approximations inherent in each calculational step are well understood and, while experts continue to debate some of the finer points, there is general consensus that the thermodynamic properties of many binary systems can now be articulated in a first-principles context.

The key assumption that makes these calculations tractable is that the atoms reside on a rigid lattice, which reduces the statistical-mechanics problem to the analysis of an Ising or generalized Ising model. For a two-dimensional system this problem may be solved by series expansions, renormalization-group analyses, transfer-matrix calculations, mean-field theory, or Monte Carlo

simulations.² For a realistic three-dimensional system only the latter two are viable options. Mean-field theory needs to go beyond the simple Bragg-Williams approximation to yield meaningful results and is usually implemented via Kikuchi's cluster variation method (CVM).^{3,4} The Monte Carlo method^{5,6} is a popular simulation technique in which excitations on a finite lattice are accepted according to a Boltzmann distribution so that the phase space of the system is sampled according to its partition function. Such excitations may either correspond to a canonical distribution (spin exchange, interchange of *A* and *B* atoms, etc.) or a grand canonical one (spin flip, replace *A* atom by *B* atom or vice versa, etc.) The CVM has the advantage that it is relatively easy to implement in a computer program and is not very demanding on computational resources. However, as a mean-field technique it has the disadvantage that it yields classical critical exponents and is not easily extended to treat interactions beyond the range of the largest cluster. For three-dimensional systems with short-range interactions it can be used to determine phase diagrams, while for two-dimensional systems it requires a bit more care, although adequate results may still be obtained. The Monte Carlo method is also fairly easy to implement, but typically consumes more computer time to ensure proper equilibration, especially near critical points, and for high-

precision work needs to be supplemented by a finite-size scaling analysis⁷ to judge or correct the effects of finite lattice dimensions. In Monte Carlo simulations one also obtains information about the kinetics of the processes involved, such as domain growth, although great care is needed to interpret the kinetics of stochastic processes and relate them to the actual kinetics of the processes being simulated. The reason for this caution is a simple one: Monte Carlo simulations are typically performed on a rigid lattice and as such, the excursions of the motif decorating the lattice in real space are not correctly tracked. For example, the interchange of two neighboring atoms on a lattice requires crossing a potential barrier with an Arrhenius-type temporal variation, modified by an attempt frequency, sometimes involving the creation of interstitials, and most likely causing a localized deformation of the surrounding lattice. None of these factors are normally included in a Monte Carlo simulation.

To obtain dynamical information about atomic scale processes (within a classical context) the most widely used computer simulation method is called molecular dynamics,^{8,9} in which, starting from some initial set of positions and momenta of all molecules or atoms, Newton's equations of motion are numerically integrated over time and the actual path of all molecules or atoms is mapped out. By taking time averages over the molecular or atomic trajectories (if so desired, after an equilibration time has elapsed) various system observables may be determined. Molecular dynamics is therefore based upon the Boltzmann formulation of statistical physics, while the Monte Carlo method follows Gibb's prescription.⁹ Molecular dynamics is well suited to describe relatively small displacements and displacive phase transformations (including nonequilibrium situations⁸), but it is less suitable for the treatment of order-disorder phase transformations because atomic or molecular *interchanges* and atomic or molecular *displacements* occur on widely different time scales.

To describe systems that undergo order-disorder transformations with a concomitant elastic deformation, it would therefore be desirable to have a technique that combines the relative ease of the Monte Carlo method with the descriptive power of molecular dynamics, and that allows the tractable study of phenomena involving the motion of atoms or molecules in complicated systems over relatively long periods of time. It is the purpose of this work to develop and implement such a methodology.^{10,11} The demonstration system chosen to investigate the effects of elastic strain associated with phase transitions in the present study is the pseudobinary high-temperature superconductor $\text{YBa}_2\text{Cu}_3\text{O}_z$ ($6.0 \leq z \leq 7.0$), although these simulation methodologies are by no means restricted to this material.

It is well established^{12,13} that oxygen plays an important role in the structure and behavior of $\text{YBa}_2\text{Cu}_3\text{O}_z$. Under appropriate thermodynamic conditions, oxygen readily diffuses in or out of the compound and may order on the oxygen-vacancy sublattice in the Cu-O basal plane. This ordering has been thoroughly studied and has been associated with the superconducting properties of the material. Although the essential plane for super-

conductivity is the CuO_2 layer, the Cu-O basal plane in an ordered state acts as a charge reservoir, thereby allowing superconductivity to persist when holes are added to or removed from the system. It has been found that a high-temperature phase transition exists in which the structure transforms from a tetragonal phase (*T*) with oxygen atoms randomly distributed on the basal plane's oxygen-vacancy sublattice, to an orthorhombic structure (*OI*) in which the oxygens in the basal plane are ordered in chains. The *OI* ground state occurs at $z=7.0$ and contains one Cu-O chain per unit cell. At very low oxygen content ($z=6.0$) the basal plane would be completely devoid of oxygen atoms, yielding another tetragonal structure. However, while a $z=6.0$ vacant phase is obtained in the simulations, the experimental structure is technically not observed in these simulations since for small oxygen concentration, oxygen atoms are also removed from other sites in the structure, most notably the so-called apical oxygen sites, and this effect cannot be described under the current two-dimensional approximation describing oxygen ordering in the basal plane. This is only a minor drawback since most of the phenomena of interest (including the occurrence of superconductivity) are associated with concentrations larger than $z \approx 6.3$ for which the apical sites are completely occupied. At concentrations between the two extremes ($6.0 < z < 7.0$) there exist a number of oxygen-ordered superstructures. There is general agreement that a cell-doubled orthorhombic phase (*OII*) occurs as a stable phase near $z=6.50$ with a ground-state structure in which every other Cu-O chain is replaced by a Cu-vacancy chain compared to the *OI* structure. The existence, as thermodynamically stable phases, of other superstructures (*OIII* in which every third chain is removed from *OI*, etc.) is still the subject of lively debate. Small regions containing such unidirectionally modulated phases have been observed experimentally and theoretical models for them have been proposed,¹⁴⁻¹⁶ but it is as yet not clear if these phases are transients or metastable inclusions. In the present work these phases will not be considered, since even if they are thermodynamically stable, they only occur in very small regions in the phase diagram and their effect on kinetics and defect structures is thought to be slight. With only *OI*, *OII*, and *T* phases present, the temperature-concentration diagram for this compound has been determined by a number of methods.¹⁷⁻²⁷ All of these works consider a static lattice and neglect elastic interactions. Nevertheless, such interactions must be present since the lattice parameters and the symmetry of the phases are different. For example, for $z=6.06$ the tetragonal phase has lattice parameters $a_0=b_0=3.8597 \text{ \AA}$,²⁸ while for $z=7.0$ at $T=300 \text{ K}$ the orthorhombic *OI* phase has lattice parameters $a_0=3.8128 \text{ \AA}$ and $b_0=3.8844 \text{ \AA}$.²⁹ Therefore, the tetragonal to orthorhombic phase transition caused by oxygen ordering is accompanied by a square to rectangular transformation of the unit cell in the basal plane indicating the presence of elastic interactions. There are also changes in the *c*-axis lattice parameter when the material undergoes this phase transition, but these will not be considered in the present paper.

A priori there are two main aspects of oxygen ordering

in $\text{YBa}_2\text{Cu}_3\text{O}_z$ wherein elasticity might be expected to play a role: phase stability and morphology. Although much effort has been devoted to the study of the microstructures and associated phase transitions in this material, many unanswered questions remain. One such question concerns the nature of the OI to T order-disorder phase transition. Many authors have suggested that the transition is second order and this is consequently borne out by calculations based upon a rigid lattice,¹⁷⁻²⁷ but a recent paper by Blagoev and Wille³⁰ shows that by considering elastic effects the transition may prove to be first order, which could explain certain conflicting experimental findings.³¹ This further highlights the need for a model incorporating elasticity to study $\text{YBa}_2\text{Cu}_3\text{O}_z$. Note that apart from changes in the order of the transitions there may also be other effects on the phase diagram and in particular that phase boundaries may be expected to shift.

Many other experimental observations for $\text{YBa}_2\text{Cu}_3\text{O}_z$ can only be explained in terms of elasticity. Such phenomena include twinning, the formation of a tweed microstructure, and deformation superstructures.³²⁻⁴⁸ Although these features have been abundantly studied experimentally, they have not received the same amount of theoretical attention that the phase diagram has. Nevertheless, it is important to investigate these defects theoretically and in a framework that allows ordering reactions concurrently with elastic deformation. For example, there is still some disagreement in the literature whether certain superstructures are stable ground states of an appropriate static Ising model or whether they are the consequence of elastic displacements. Therefore, a theoretical framework is needed that disentangles the ordering and the elastic contributions to the total energy.

Recently, two other distinct theoretical treatments based on paradigms different from that in the present paper have described aspects of the elastic behavior of $\text{YBa}_2\text{Cu}_3\text{O}_z$. Semenovskaya and Khachatryan⁴⁹⁻⁵¹ analyze the kinetics of ordering in this material taking into account elastic strain. They use a microscopic diffusion equation in combination with a mean-field approximation for the free energy to derive an equation giving the probability of finding an oxygen atom on a given site as a function of time. This equation is solved in reciprocal space and after back transformation may be used to construct photographs illustrating the state of the system at a given time. These photographs are produced by indicating an oxygen atom on a given site when that site's occupation probability is greater than or equal to the overall oxygen concentration, and placing a vacancy on that site otherwise. This technique reproduces many of the experimentally observed defects such as tweed morphologies and twin boundaries. In another study of strain, restricted to $\text{YBa}_2\text{Cu}_3\text{O}_7$, Parlinski and co-workers⁵²⁻⁵⁴ use a two-dimensional molecular dynamics simulation to model strain coupling via fixed displacements associated with oxygen occupancy in the basal plane of this phase. The atoms are assumed to be connected by harmonic springs and the occupation variables on the oxygen/vacancy sublattice (normally restricted to be either +1 or -1) are taken as continuous variables.

A study of quenching found that tweed patterns rapidly formed, followed by a coarsening leading to a microtwinning structure, which after further annealing eventually led to a single domain. This approach was recently extended⁵⁵ to off-stoichiometric compositions of $\text{YBa}_2\text{Cu}_3\text{O}_z$ ($z < 7.0$) and produced some very enlightening photographs of tweed and microtwinning domains. It was found that oxygen vacancies tended to gather along the domain walls which led to a slowing down of the annealing kinetics, even though the OII phase (and other modulated phases) were not included as stable ground states in the underlying Hamiltonian.

In contrast to these approaches, the present work uses a more general treatment based upon a real-space statistical description combined with first-principles interaction parameters. Occupation variables only take on discrete values (+1 for an oxygen, -1 for a vacancy), while atoms may be displaced from their initial positions in small steps with a resolution limited only by the numerical accuracy of the computer used in the simulations. This enables the exploration of a quasicontinuous variation of overall oxygen concentration ($6.0 \leq z \leq 7.0$) and atomic positions in the basal plane of $\text{YBa}_2\text{Cu}_3\text{O}_z$ and permits the determination of photographs that may be directly compared with experiment. The underlying statistical physics model is the stress ensemble in which atomic positions are *free* variables of the system. Such a treatment closely mirrors reality and allows the direct determination of structural information, both in real space and in reciprocal space, as a complement to experimental characterization. The combination of first-principles calculations and direct experimental measurement makes possible an unambiguous determination of model parameters, promising true predictive capacity for a variety of materials. Although initially applied to $\text{YBa}_2\text{Cu}_3\text{O}_z$, the approach is generally valid and may in the future be used to study other systems displaying martensitic or displacive transformations in multicomponent systems where soft mode phonon behavior is important.⁵⁶

II. MODEL

As outlined in the previous section, the objective of the current work is to include elasticity in Monte Carlo simulations of phase transformations in the basal plane of $\text{YBa}_2\text{Cu}_3\text{O}_z$. To accomplish this, the asymmetric next-nearest-neighbor Ising (ASYNNNI) model first proposed by de Fontaine, Wille, and Moss⁵⁷ for the study of oxygen ordering in this system needs to be extended. In spite of its simplicity, this model has been very successful in describing the phase diagram and defect structures of the actual material.¹⁷⁻²⁷ In particular, using the CVM, Monte Carlo, or transfer-matrix methods, in combination with first-principles interaction parameters,^{20,23} excellent agreement with the experimentally accessible portions of the phase boundaries is obtained. Nevertheless, a number of features cannot be described by a static model. Clearly, the crucial element that is missing in this treatment is the elastic contribution to the free energy.

Through the inclusion of elastic interactions, the present study extends the ASYNNNI static lattice model by using the strict harmonic approximation. The use of

this approximation is justified by the fact that all displacements are small and by the work of Pyka *et al.*⁵⁸ and Schweiss *et al.*⁵⁹ who did not find evidence for strong anharmonicity in $\text{YBa}_2\text{Cu}_3\text{O}_z$. The harmonic approximation is, however, not essential for the general methodology and one can easily go beyond it in cases where this is needed. To introduce strain effects, the complete interatomic potential, J , is expanded in a Taylor series to second order for each of the interacting pairs, n , such that,

$$J_n = (0; E_{LMNK}) + \left. \frac{\partial J(\mathbf{r}; E_{LMNK})}{\partial r_n} \right|_{r=0} \times dr_n + \left. \frac{1}{2} \frac{\partial^2 J(\mathbf{r}; E_{LMNK})}{\partial r_n^2} \right|_{r=0} dr_n^2 + \dots \cong V_n + k_n(r_n - r_{0,n})^2, \quad n \in \{1, 2, 3\}, \quad (1)$$

where V_n are the effective pair interactions (EPI's) which may be calculated from first principles:¹ V_1 acts between nearest-neighbor oxygen-vacancy sites, V_2 between next-nearest sites through an intervening copper, and V_3 between next nearest neighbors without an intervening copper; $r_{0,n}$ are the equilibrium spacings in an appropriate reference state between the two sites interacting via V_n ; E_{LMNK} is the appropriate strain tensor component; r_n are the actual spacings; and k_n are spring constants for each pair (see Fig. 1 in Ref. 10). The first-order term in the Taylor expansion is necessarily zero in accordance with equilibrium conditions. Using the $z=7.0$ orthorhombic configuration (OI) at 300 K as the reference strain state²⁹ from which the equilibrium spacings are obtained, the spring constants are derived from the set of elastic constants⁶⁰ acting in the basal plane via

$$C_{LMNK} = \frac{2}{\Omega_0} \sum_{i=1}^N \sum_{j \neq i}^N \left. \frac{\partial^2 J_{ij}(r(i,j))}{\partial r(i,j)^2} \right|_0 \Delta X_L(i,j) \Delta X_M(i,j) \Delta X_N(i,j) \Delta X_K(i,j), \quad (2)$$

as outlined by Weiner.⁶¹ Here Ω_0 equals the volume of a unit cell, ΔX_l ($l=L, M, N, K$) is the difference in Lagrangian coordinates between atom i and atom j in the l th direction, and the summations are over all N atoms in the unit cell. To allow coupling of the copper and oxygen sublattices, the k_2 constant is divided into two components where each acts between either a copper and an oxygen ($k_{2,o}$) or a copper and a vacancy ($k_{2,v}$).

The system is therefore described by the grand canonical stress ensemble, $\Lambda(T, P, \mu, \sigma_{lmnk})$, with the Hamiltonian

$$H = \sum_i^N \left[\sum_j^{\text{NN}} \{V_1 \sigma_i \sigma_j + k_1 [r_{ij} - r_{0,1}]^2\} + \sum_j^{\text{NNN}''} \{V_2 \sigma_i \sigma_j + k_2(\sigma_i) [r_{\text{Cu},i} - r_{0,2}(\sigma_i)]^2 + k_2(\sigma_j) [r_{\text{Cu},j} - r_{0,2}(\sigma_j)]^2\} + \sum_j^{\text{NNN}'''} \{V_3 \sigma_i \sigma_j\} + \mu_i \sigma_i \right], \quad (3)$$

where the outer summation is over all N oxygen-vacancy sites, σ is an Ising spin variable whose value takes on ± 1 signifying either an oxygen or vacancy, respectively, and μ is the oxygen chemical potential [related to oxygen partial pressure through: $\mu' = \mu_0 + \ln(p_{\text{O}_2})$]. The designations NN, NNN, and NNN'' indicate summations over nearest-neighbor pairs, next-nearest-neighbor pairs through an intervening copper cation, and next-nearest-neighbor pairs with no intervening copper on the oxygen-vacancy sublattice, respectively. (Fig. 1 in Ref. 10). With all spring constants set to zero, this Hamiltonian reduces to that of the ASYNNNI model.

The Hamiltonian (3) belongs to a class of models sometimes designated as compressible Ising models.^{5,62,63} Such models have been studied previously, mainly by Landau theory,⁶⁴ but they have not received a great deal of attention by direct computer simulation. Some authors⁶² have treated the elastic degrees of freedom by introducing multispin interactions reducing the problem to an effective static lattice Ising Hamiltonian. However, in the present work the aim is to treat the elastic degrees of freedom explicitly by allowing for atomic displacements away from nominal lattice sites.

Effective pair interactions, such as those occurring in

(3), have been well studied in theories of alloy formation and stability.¹ In the present work, concentration-independent interactions obtained by the Connolly-Williams method are used. These were determined by Sterne and Wille^{20,23} from first-principles band-structure calculations based on the linearized muffin-tin orbital method within the atomic sphere approximation (LMTO-ASA). These EPI's have been used in a number of calculations of the phase diagram^{20,21,23} and, in general, agreement with experiment is very good. Hilton *et al.*²⁵ have taken experimental phase boundary data and through an inversion procedure based on transfer-matrix analysis determined the EPI's (within the ASYNNNI model) that would give rise to these transition lines. They find a modified set of interactions that naturally gives a better fit. However, the agreement with the first-principles EPI's is quite good, certainly if one takes into account the simplifications inherent in the model itself (static lattice, two-dimensional system, pair interactions only, interactions restricted to first and second neighbors, etc.) as well as those inherent to the electronic structure calculation (ASA, local-density approximation, etc.).

It is not possible to extend the Connolly-Williams

method to obtain spring constants simultaneously with EPI's from first principles because this method relies on a cancellation of errors for which it is essential that all calculations are performed with the same Brillouin zone. In the present work, a direct approach is used to obtain the spring constants based on a fit to elastic parameters. By application of Eq. (3) and a knowledge of the elastic constants acting in the basal plane of $\text{YBa}_2\text{Cu}_3\text{O}_z$, one can derive numerical values for the spring constants, k , used in the Hamiltonian (3) for this model. For the orthorhombic phase, there are four elastic constants acting only within the basal plane of this material: C_{11} , C_{22} , C_{12} , and C_{21} . For this model, there are also four spring constants: k_1 , $k_{2,0}$, $k_{2,v}$, and k_3 . The spring constants acting within the oxygen-vacancy sublattice, k_1 and k_3 , are *effective spring constants*, analogous to effective pair interactions. In particular, they have the form

$$k_{n,\text{eff}} = k_{n,0-v} - \frac{(k_{n,0-0} + k_{n,v-v})}{2}, \quad (4)$$

where $k_{n,0-0}$ is the spring constant acting between oxygen positions and $k_{n,v-v}$ is the spring constant acting between vacancy position, the subscript n designating the range of the constant. The $k_{2,0}$ and $k_{2,v}$ spring constants, which act between the copper and oxygen-vacancy sublattices, are true spring constants. By use of Eq. (4) and application of Eq. (2) to a model unit cell of the *OI* phase with the reference lattice constants at the reference temperature and considering the choice of spring constants in this model, one arrives at four equations for four unknowns and the derivation of numerical values for the spring constants can be made.

The Hamiltonian (3) may be studied by a number of techniques from statistical mechanics. Landau theory is very useful to obtain general information about the nature of the phase transitions, but does not lend itself easily to produce more detailed information such as a full phase diagram or kinetics. The CVM is not readily extended to include displacements. One would have to incorporate both correlation functions and lattice positions as variables in the free energy and this would lead to a very complex minimization problem with a large number of degrees of freedom. Alternatively, one could make certain simplifying assumptions about the nature of the displacements to reduce the size of the minimization problem. Such formalisms have recently been proposed^{65,66} and appear quite promising, but there is not as yet sufficient experience to evaluate their applicability. An additional complication is that there is no unique way to include vibrational entropy into this formalism. Instead, one could use the mean-field approach of Semenovskaya and Khachatryan⁴⁹⁻⁵¹ and include elastic interactions into the Hamiltonian, but without allowing any actual displacements of atoms from their sites and using occupation probabilities (rather than actual occupancies) as dynamic variables. Although this method produces photographs that are very enlightening, there are obvious advantages to having a method that tracks atoms in real space during their dynamic evolution. Molecular dynamics simulations also give valuable infor-

mation about the kinetic behavior of the system, but are less suited for cases where order-disorder and displacive transformations occur simultaneously. A possible approach is that championed by Parlinski and co-workers⁵²⁻⁵⁵ through the use of continuous occupation variables, but again, in spite of some very elucidating insights, the simulated order/disorder reaction does not correspond to any actual physical process. Therefore, an ordering reaction with an associated strain field is readily and naturally described by the Monte Carlo method.^{5,6}

The Monte Carlo simulations in this work are performed in the grand canonical stress ensemble. Two types of Monte Carlo excitations are needed in the simulation to employ the Hamiltonian described above for this system. These involve changes in oxygen occupancy (only on the oxygen-vacancy sublattice) and small displacements of particles on both sublattices (oxygen-vacancy and copper). All excitations are performed with Glauber dynamics in which the thermodynamic intensities (i.e., chemical potential and stress) are held constant while the corresponding thermodynamic coordinates (i.e., oxygen concentration and strain, respectively) are not conserved. These excitations have associated with them a change in energy ΔH , and the corresponding move is accepted according to the standard Metropolis criterion,⁵⁻⁶ if the Boltzmann factor $\exp(-\Delta H/k_B T)$ is larger than a random number chosen from the interval [0,1]. Since first-principles interactions are used, it is possible to convert simulation temperature to absolute temperature as will be done for all results reported in this paper. Based upon experience with the static ASYNNNI model, it is to be expected that these absolute temperatures are in reasonable agreement (approximately within 20%, which is quite satisfactory for a parameter-free calculation) with the experimental temperature.

The question of boundary conditions becomes an important issue in the implementation of the model. Free boundary conditions lead to significant edge artifacts and limit the simulation to very small sample sizes. Conversely, periodic boundary conditions, although still somewhat artificial, are ideal in that no edge effects are present and are commonly used in static lattice Monte Carlo simulations. However, with displacive excitations present, the simulation of periodic boundary conditions is much more difficult to achieve while still maintaining volume as a free variable. In the present work periodic boundary conditions are implemented in a manner which allows volume changes in the system, akin to the Parrinello-Rahman technique in molecular dynamics.⁶⁷ Free-volume yet periodic boundary conditions are accomplished by segregating the displacive Monte Carlo excitation step into two components: one performed upon a reference lattice for all the atoms in the system (which results in changes in volume of the lattice), and one performed upon the local Lagrangian coordinates of each particle relative to the reference point. The Eulerian coordinate of any atom is then the sum of the Lagrangian coordinate and the corresponding multiple, labeling the atom, of the current lattice parameter in the [100] or [010] direction (Fig. 1).

Another issue that arises in determining the simulation

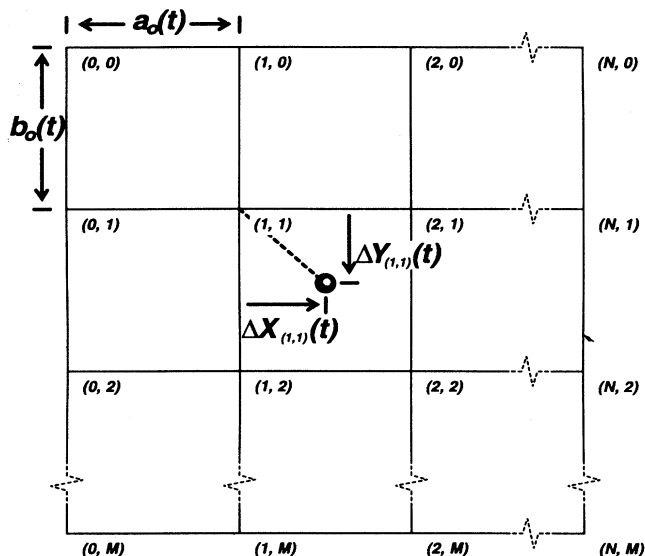


FIG. 1. Schematic illustrating implementation of free-volume periodic boundary conditions. Each site has both reference lattice coordinates and Lagrangian coordinates (ΔX and ΔY) relative to the reference lattice position.

parameters is the normalization of the excitation steps. Ideally for every ordering step that occurs there should be a relaxation of the lattice parameters and a subsequent relaxation of all atomic positions. However, this would incur a great amount of computer time and may not even be necessary for the purposes of elucidating the phase diagram and typical defect structures. Therefore, for this study, for every ordering step that occurs, there is an excitation of the lattice parameter in the a direction, an excitation of the lattice parameter in the b direction, 10 local shifts of copper atoms, and 20 local shifts of oxygen or vacancy particles (normalized to take into account the two-to-one ratio of oxygen-vacancy sites to copper sites). In the remainder of this paper, simulation times are reported in terms of Monte Carlo steps per particle (MCSP), where 1 MCSP is the combination of excitation attempts described above.

III. RESULTS AND DISCUSSION

A. Comparison to ASYNNNI model without elasticity

Clearly, it is important to determine whether the present model, which includes elasticity, appropriately describes the $\text{YBa}_2\text{Cu}_3\text{O}_z$ system by stabilizing the experimentally observed structures and predicting the phase transitions between them. It is also of interest to determine which, if any, effects elasticity has on the results previously obtained with static models. Although it is not the primary focus of the present study, some phase diagram information was obtained in the course of investigating defect structures, as will now be discussed. However, these results must be taken as indicative of possible trends, rather than representing an exhaustive study,

since no attempt was made to find accurate phase boundaries by going to very long runs with proper equilibration times and accurate statistics, nor were finite-size effects addressed by a scaling analysis. Nevertheless, a number of conclusions can be unambiguously made.

Extending previous arguments^{68,69} for the static ASYNNNI model, it is easy to see that the model described by the Hamiltonian (3) contains OI and OII as stable ground states (at zero temperature), provided that $V_1 > 0$, $V_2 < 0$, and $0 < V_3 < V_1$. Such is indeed the case for the first-principles parameters used here. It was also found in the Monte Carlo simulations that the current model does contain the commonly observed orthorhombic structures in $\text{YBa}_2\text{Cu}_3\text{O}_z$ at finite temperature with phase transitions between the two orthorhombic phases and between them and the tetragonal phase. Typical photographs of the OI, OII, high-temperature tetragonal, and oxygen-depleted tetragonal phases obtained in this study are depicted in Fig. 2.

Although the commonly observed oxygen-ordered structures are predicted by both the ASYNNNI model without elasticity and the present model with elasticity included, the stability regions of these phases were found to differ. Figure 3 shows plots of concentration versus chemical potential for the two models at the same constant temperature ($T=330$ K). Both models find all

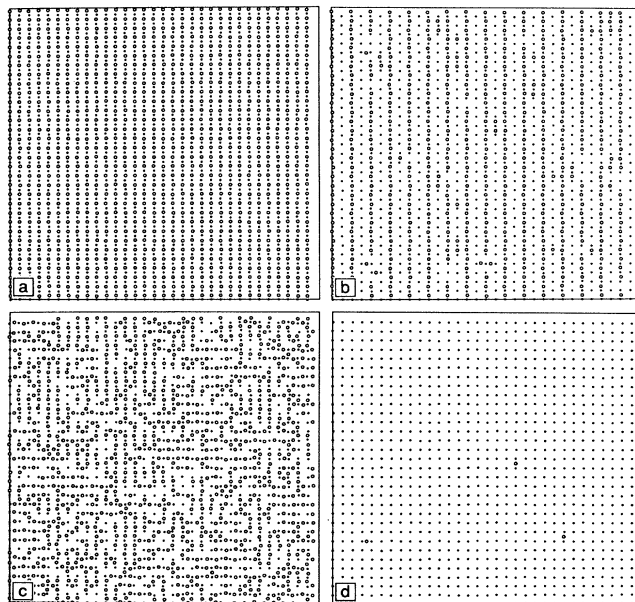


FIG. 2. Representative photographs of equilibrium phases. (a) Orthorhombic I with $a_0=3.812$ Å and $b_0=3.885$ Å obtained after 12 000 MCSP at $T=330$ K and $\mu=-4.0E-20$ J; (b) Orthorhombic II with $a_0=3.819$ Å and $b_0=3.854$ Å obtained after 15 000 MCSP at $T=330$ K and $\mu=-6E-20$ J; (c) high-temperature tetragonal with $a_0=3.827$ Å and $b_0=3.823$ Å obtained after 6000 MCSP at $T=2640$ K and $\mu=0.0$ J; and (d) low oxygen content tetragonal with $a_0=3.835$ Å and $b_0=3.839$ Å obtained after 10 000 MCSP at $T=330$ K and $\mu=-8.0E-20$ J.

three phases (*OI*, *OII*, and *T*) to exist at this temperature for different values of the chemical potential, μ , i.e., for different concentration ranges. However, as can be seen in Fig. 3 the width of the stability region of *OII* has diminished considerably with the inclusion of elasticity in the model. This observation is in agreement with experiment³⁷ which finds *OII* to occur over a smaller concentration range than was previously calculated based on the static lattice ASYNNNI model.^{21,23}

The phase transitions that are known to occur between these structures were found to be correctly located by the present study. Figure 4 shows a plot of specific heat versus temperature for $\mu=0.0J$. The data for each point were obtained for lattices composed of 16×16 unit cells averaged over 10 000 MCSP once the simulation had sta-

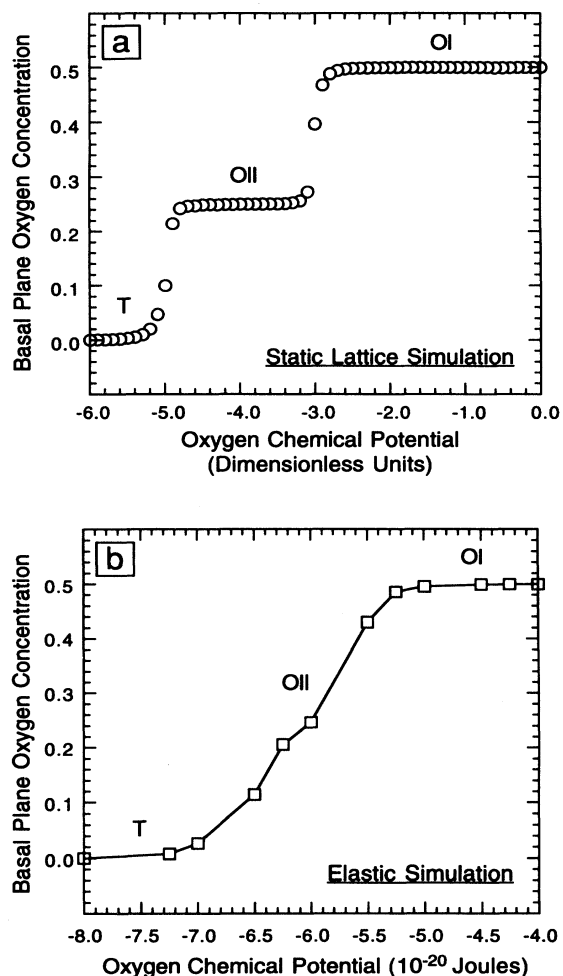


FIG. 3. (a) A plot of concentration versus chemical potential at 330 K for the ASYNNNI model without elasticity. Plateaus indicative of the *OI*, *OII*, and *T* stability regimes can clearly be seen. (b) A plot of concentration versus chemical potential at 330 K for the present model which includes elasticity. The *OI*, *OII*, and *T* regimes can be seen; however, the *OII* plateau is clearly much smaller than in Fig. 3(a) (without elasticity).

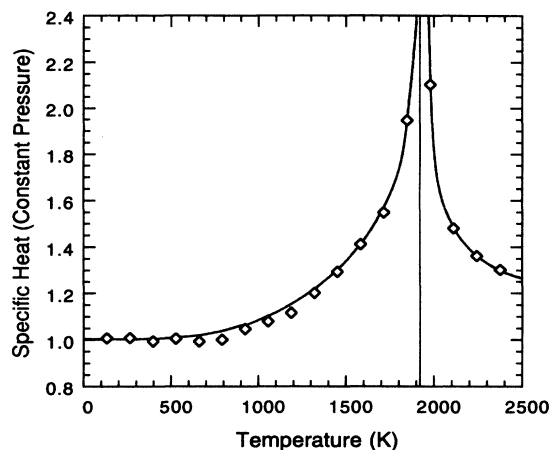


FIG. 4. A plot of specific heat versus temperature at a constant chemical potential of 0.0J. A peak can be seen at approximately 1920 K which represents the orthorhombic to tetragonal phase transformation.

bilized to equilibrium under the given thermodynamic conditions. A peak in the curve indicative of the orthorhombic-tetragonal phase transition can be clearly seen at approximately 1920 K. However, longer runs for larger lattices are needed to pinpoint the exact location and nature of the phase transition.

Finally, there is the earlier mentioned possibility that in the presence of elastic interactions the *OI-T* transition may become first order, as suggested in the Landau-theoretical analysis of Blagoev and Wille.³⁰ The numerical evidence from the present simulations is that if there is coexistence it occurs over a narrow region in the phase diagram. However, the current search has focused mainly on the defect structures and a further detailed study (including runs for larger lattices) is necessary to investigate possible first-order transitions. In view of the overwhelming experimental evidence for coexistence (quoted in Ref. 30; see also Ref. 31), if elasticity is not borne out as the underlying cause, other mechanisms must be sought, such as repulsive further-neighbor interactions as suggested by Günther, Rikvold, and Novotny.⁷⁰ Note that a Landau-theory analysis (as performed in Ref. 30) can only suggest the possibility of a first-order transition, not prove that it must occur.

Thus, the current model correctly describes the overall behavior known to be present in $YBa_2Cu_3O_2$. The oxygen-ordered phases as well as the transitions between them which were found to exist within the ASYNNNI model are also found to exist within the present model with elasticity included. However, it was observed that the addition of elasticity leads to results (narrower stability region for *OII*) which are in better agreement with experimental observations than results previously obtained. In addition, the new model with elasticity is able to include phenomena which are caused by strain and which the ASYNNNI model without elasticity could therefore not describe. These phenomena such as deformation su-

perstructures, tweed, and twinning are known from experiment to occur in $\text{YBa}_2\text{Cu}_3\text{O}_z$ and are discussed in the following sections. Some of these results have also briefly been presented elsewhere.^{10,11}

B. $n\sqrt{2}a \times m\sqrt{2}a$ superstructures

There have been numerous reports³²⁻³⁶ of superstructures in $\text{YBa}_2\text{Cu}_3\text{O}_z$ with lattice parameters equal to a multiple of $\sqrt{2}a_0$. Specific examples of such unit cells include $\sqrt{2}a_0 \times \sqrt{2}a_0$, $2\sqrt{2}a_0 \times 2\sqrt{2}a_0$, and $\sqrt{2}a_0 \times 2\sqrt{2}a_0$. These structures have been studied using a variety of characterization techniques and their existence is well confirmed. However, there is little consensus on the mechanism or structure responsible for the $\sqrt{2}$ phases, with the exception that most explanations do appeal in part to the elastic properties of $\text{YBa}_2\text{Cu}_3\text{O}_z$. Published theories for the origin of the $\sqrt{2}$ superstructure include a barium deficiency,³² cooperative displacements of copper cations in the basal plane,³⁵ equilibrium structures arising from long-range interactions,⁷¹ oxygen-ordered superstructures,^{36,72} or modulated Jahn-Teller distortions involving the CuO_2 layer.⁴³ It must be mentioned that the explanation of these structures in terms of long-range interactions has been questioned⁷³⁻⁷⁵ and that most authors accept that such interactions may lead to uniaxially modulated phases (*OIII*, etc.) but not to the $\sqrt{2}$ superstructures. This is also confirmed by recent first-principles calculations.⁷⁶

As the $\sqrt{2}$ superstructures are typically produced by heating and subsequent cooling through the *T-O* transition,^{35,36} a simulation sample of 1024 unit cells was disordered at 2700 K and then cooled to and annealed at 330 K at an oxygen partial pressure yielding $z=7.0$ after complete oxygen ordering into the *OI* phase.¹⁰ After annealing for 4000 MCSP, a $\sqrt{2}a_0 \times \sqrt{2}b_0$ superstructure similar to that observed in electron diffraction by Chen *et al.*³⁴ was observed to form (Fig. 2 in Ref. 10). Figure 2(a) in Ref. 10 depicts a photograph of a lattice with the $\sqrt{2}a_0$ structure obtained after this annealing treatment. The existence of the superstructure in the simulation photograph was confirmed by examining the fast Fourier transform (FFT) intensities of the lattice configuration. The $(h/2, k/2, 0)$ superlattice reflections indicative of the $\sqrt{2}a_0 \times \sqrt{2}a_0$ superstructure could be clearly seen [Fig. 2(b) in Ref. 10]. By enlarging a section of the simulation photograph [see box and corresponding enlargement in inset of Fig. 2(a) of Ref. 10], the mechanism responsible for the origin of the $\sqrt{2}$ superstructure could be exam-

ined. It was found that the positions of oxygen atoms in the ordered O-Cu-O chains running in the [010] direction were being modulated by a transverse wave of period $2a_0$, deflecting the positions of oxygens from their *OI* equilibrium positions alternatively in the [100] or $[\bar{1}00]$ directions. Moreover, the displacement wave was 180° out of phase in adjacent O-Cu-O chains.

To better characterize the $\sqrt{2}a_0$ phase, the atomic positions of Fig. 2(a) of Ref. 10 were statistically examined. Vacancies, which are treated as particles in the simulation, were seen to displace in an analogous manner to the oxygens, but with the transverse displacive wave running along the [100] direction, affecting the Cu-vacancy chains. The cooperative displacements of both the oxygens and vacancies together yield the $\sqrt{2}a_0 \times \sqrt{2}a_0$ superstructure. The average net and absolute values of the displacements for the three species are given in Table I. From the values in this table it is clear that the modulations which give rise to the $\sqrt{2}a_0 \times \sqrt{2}a_0$ structure are confined to the oxygen-vacancy sublattice. The average displacements of all sites (oxygen, vacancy, and copper) are very similar and are very small ($< 0.10 \text{ \AA}$), simply an indication of a small overall shift in the simulation lattice relative to its reference origin. By examining the average of the absolute value of the displacements it can be seen that the displacements are small for the copper atoms in both directions, for the oxygen atoms in the [010] direction (along the O-Cu-O chains), and for the vacancies in the [100] direction. However, the average absolute value of the displacements of the oxygens perpendicular and vacancies parallel to the Cu-O chains are significant ($\approx 0.20 \text{ \AA}$). The observation that the average absolute value of the displacements is finite while the average net value is equal to the reference lattice shift indicates that these modulations occur about the equilibrium positions of the oxygen and vacancy sites in the ordered *OI* plane. The net effect of particle displacements is succinctly described by a $\mathbf{q} = [\frac{1}{2}, \frac{1}{2}, 0]$ wave vector on the oxygen-vacancy lattice which has the effect of rotating the *OI* lattice vectors by 45° , resulting in lattice parameters of approximately $\sqrt{2}a \times \sqrt{2}a$ [$a \approx (a_0 + b_0)/2$] [inset of Fig. 2(a) of Ref. 10].

To investigate the evolution of the $\sqrt{2}$ structure, strain maps corresponding to individual simulation photographs were obtained by plotting the radial displacement from equilibrium of each atom on a 256 gray scale plot with white representing the maximum strain and black representing the minimum strain in the lattice.¹¹ The strain map corresponding to Fig. 2(a) of Ref. 10 exhibited

TABLE I. Displacements from equilibrium position for various sites.

Site type	Average displacement from equilibrium (\AA)			Average of absolute value of displacement from equilibrium (\AA)	
	x	y	r	x	y
Copper	0.0719	-0.0262	0.103	0.0777	0.0540
Oxygen	0.0711	-0.0285	0.224	0.0748	0.2060
Vacancy	0.0718	-0.0289	0.212	0.2010	0.0505

a distinctive pattern of contrast superposed over diffuse background strain. This contrast consists of small nearly circular regions (about 8 Å in diameter) organized into a square array oriented at an angle of 45° to the lattice boundaries. By performing strain image simulations, it was confirmed that the $\sqrt{2}a_0 \times \sqrt{2}a_0$ superstructure results in this distinctive strain contrast pattern (Fig. 5). This $\sqrt{2}$ strain pattern is seen to be uniformly distributed throughout the strain map, indicating that the $\sqrt{2}a_0 \times \sqrt{2}a_0$ superstructure is present throughout the entire simulation sample of Fig. 2(a) in Ref. 10.

Next, a set of simulations was performed with the aim of separating the contribution of strain from that of

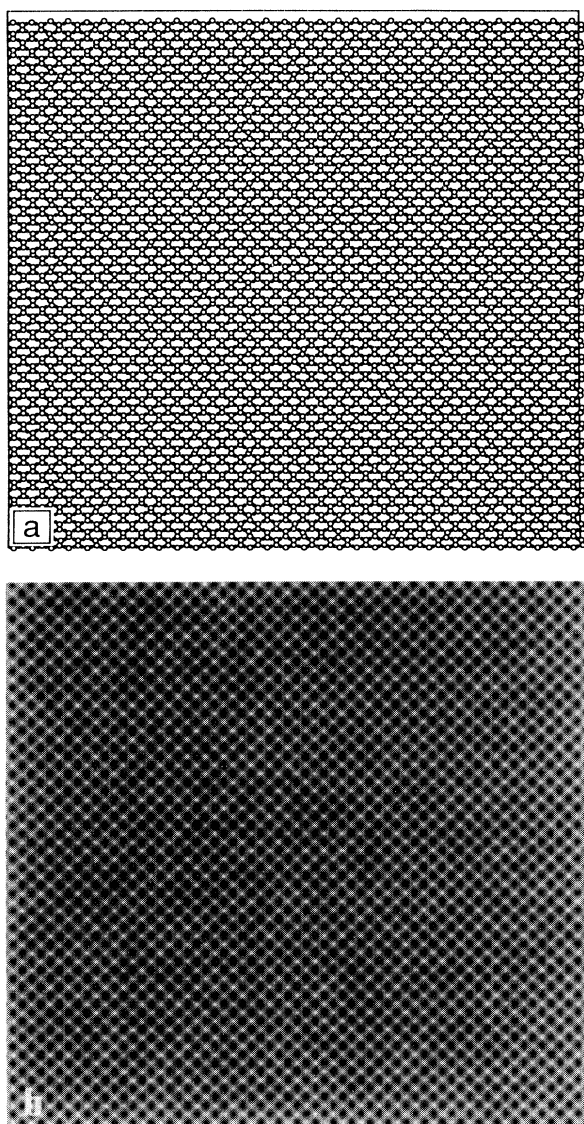


FIG. 5. Simulation of the $\sqrt{2}$ structure. (a) Idealized photograph of the $\sqrt{2}$ superstructure. (b) Simulated strain map of the $\sqrt{2}$ structure based on the photograph of (a).

oxygen-vacancy ordering to the formation of the $\sqrt{2}a_0 \times \sqrt{2}a_0$ structure and to investigate its dynamic stability. To this end an ordered *OI* configuration of 32×32 unit cells was deformed such that it had tetragonal symmetry with $a = 3.8541$ Å and then annealed at a temperature of 660 K and a chemical potential of 0.0J (in the *OI* regime of the phase diagram). Figure 6 shows a sequence of FFT intensities of the lattice after 1000, 4000, 7000, and 10 000 MCSP. The $\sqrt{2}a_0 \times \sqrt{2}a_0$ superlattice spots can be seen to appear diffusely, to sharpen, to disappear, to reappear diffusely, to resharpen, etc. This suggests that the displacements leading to the $\sqrt{2}$ superstructure are dynamic rather than static. Such findings are consistent with those reported by Pyka *et al.*⁵⁸ who performed inelastic neutron scattering to study *ab*-plane polarized transverse chain-oxygen vibrations in $\text{YBa}_2\text{Cu}_3\text{O}_z$. A mode was found at $\mathbf{q} = (\frac{1}{2} \frac{1}{2} 0)$ which is equivalent to the resultant of the displacements found here to be responsible for the $\sqrt{2}a_0 \times \sqrt{2}a_0$ superstructure. Pyka *et al.*⁵⁸ further observed that this mode is dynamical with a frequency on the order of 5 THz. By plotting the net displacements of oxygen atoms along the [100] direction and vacancies along the [010] direction as a function of simulation time (Fig. 7), the dynamic and periodic nature of the $\sqrt{2}$ structure is clearly apparent. The period of the oscillation in simulation time is approximately 16 000 MCSP.

What is of particular interest here is that the $\sqrt{2}$ super-

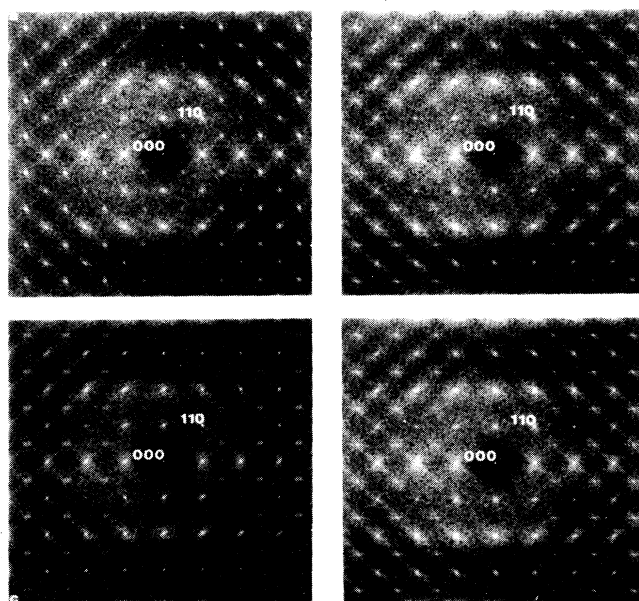


FIG. 6. A time sequence of FFT's obtained after annealing a 32×32 unit-cell artificially deformed tetragonal lattice at 660 K and a chemical potential of 0.0J for (a) 1000 MCSP, (b) 4000 MCSP, (c) 7000 MCSP, and (d) 10 000 MCSP. The $\sqrt{2}a_0 \times \sqrt{2}a_0$ superlattice reflections can be seen to appear diffusely (a), to sharpen (b), to disappear (c), and to reappear diffusely (d), indicating a cycling of the phase.

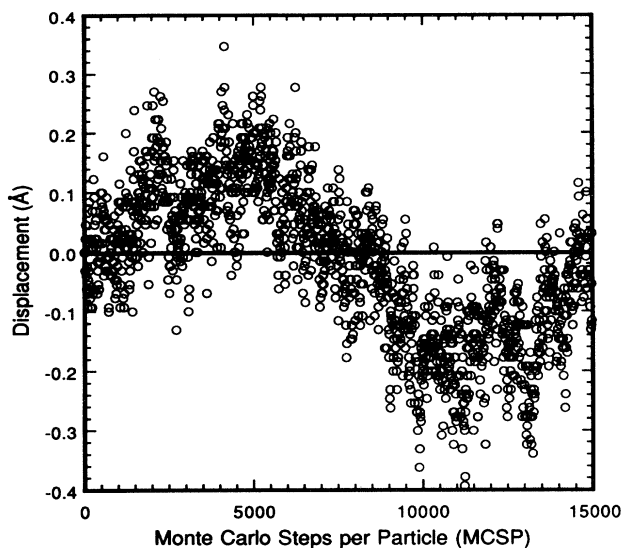


FIG. 7. Oxygen-vacancy displacements vs simulation time illustrating the dynamic nature of the phonon wave giving rise to the $\sqrt{2}$ structure.

structure arises purely from strain effects rather than being due to some additional oxygen-vacancy ordering. Such findings strongly suggest that the $\sqrt{2}$ superstructure represents a mode in which the system can dissipate excess strain energy via a phonon mode with wave vector $\mathbf{q} = [\frac{1}{2} \frac{1}{2} 0]$. Such a scenario would be consistent with mode softening, which is typically associated with a symmetry operator lost during a transformation. Since the (110) mirror plane is lost in the tetragonal to orthorhombic transition in this system, mode softening with wave vector $\mathbf{q} = [\frac{1}{2} \frac{1}{2} 0]$, as is suggested here, is consistent with the loss of symmetry associated with the order-disorder transformation in this system. In addition, the tetragonal-orthorhombic transformation in the material is generally held to be of second order and it is common for such a transformation involving strain to display phonon-softening behavior. Moreover, it is quite likely that similar modulations on other oxygen-ordered (oxygen-deficient) superstructures (which Adelman *et al.*¹⁶ have shown to exist as a devil's staircase) will yield analogous deformation superstructures. However, these devil's staircase phases (OIII, etc.) are not stabilized in the present Hamiltonian with only first and second neighbor interactions. At lower oxygen stoichiometries, families of $n\sqrt{2}a_0 \times m\sqrt{2}a_0$ superstructures (n, m are integers) have been observed in numerous experimental studies³²⁻³⁶ and also (for $n = m = 2$) in the simulations of Semenovskaya and Khachatryan.⁴⁹⁻⁵¹ It seems very likely that these larger $\sqrt{2}$ superstructures arise via an analogous mechanism to the $n, m = 1$ case observed here but with a longer transverse wavelength so as to be commensurate with the larger unit-cell dimensions of the ordered phases occurring at lower oxygen contents. Work is in progress to see if deformation superstructures do in

fact result from such modulations within the present model.

Finally, the role of elasticity is thought to be critical to the origin of the $\sqrt{2}$ superstructures for two reasons: (1) theories based on static oxygen-ordering mechanisms alone must rely on increasingly complicated models involving numerous and increasingly unphysical pair interactions, and (2) the experimental observations that the $\sqrt{2}$ superstructures are the product of cooling treatments which in and of themselves impose thermal stresses on the system in addition to the large stresses associated with the tetragonal to orthorhombic transition. Only those models that take into account both the compositional and elastic aspects of the system behavior, such as the one investigated here, have the capability to provide a complete, unified, and concise explanation for all the phenomena observed, both kinetic and equilibrium.

C. Tweed

In an investigation of the basket-weave or tweed contrast arising in electron micrographs, it is first useful to distinguish between two distinct tweed contrasts. The actual basket-weave tweed contrast is a fine scale (tens of angstroms) deformation microstructure occurring in completely oxygen-ordered domains. A second form of tweed contrast is that arising from the strain associated with domain boundaries, typically twin boundaries occurring in this system. This domain boundary contrast is on a much larger scale (tens of nanometers). In the present theoretical study, the fine-scale deformation microstructure will be referred to as tweed texture, whereas the domain contrast will be distinguished as domain tweed.

Several previous theoretical studies⁴⁹⁻⁵⁵ of elasticity and oxygen ordering in $\text{YBa}_2\text{Cu}_3\text{O}_z$ have produced lattice configurations that indicated the presence of tweed. Using the present model, abundant evidence of the tweed microstructure was also observed during the tetragonal to orthorhombic phase transition in this material. Since the other theoretical studies⁴⁹⁻⁵⁵ made certain simplifying assumptions about the nature of the occupation variables, it appears that the exact details of the site occupancies are not important to produce this effect and that it should be possible to observe it in a fully ordered, tetragonal (and thus strained) sample. This was indeed borne out by the present simulations.

As mentioned before, in the investigation of the $\sqrt{2}$ superstructures, a fully oxygenated ($z = 7.0$), oxygen-ordered sample consisting of 32×32 unit cells was strained such that $a_0 = b_0 = 3.8541 \text{ \AA}$. The resulting configuration was then allowed to anneal at a temperature of 660 K and a chemical potential of 0.0 J (inside the OI stability region). The initial response of the system to the imposed strain was the formation of the $\sqrt{2}a_0 \times \sqrt{2}a_0$ superstructure as discussed in the preceding section. However, as time progressed, a tweed structure clearly appeared. Evidence of this can be seen in the FFT intensities of the lattice configuration [Fig. 6(d)] resulting after annealing for 10 000 MCSP. Cross streaking in the $\langle 110 \rangle$ directions can be observed about the diffraction spots. Contour plots of the (300) reflections

for each of the FFT's of Fig. 6 are given in Fig. 8 to facilitate the observation of the cross streaking. Schwarz *et al.*³⁷ present a similar contour plot of the (010) reflection. This $\langle 110 \rangle$ streaking is the hallmark of tweed. In addition, the streaking appears to lengthen as the order of the reflection increases in agreement with the observations of Zhu and co-workers³⁸⁻⁴⁰ and Lacayo and Kästner.⁴¹

Streaking in the $\langle 110 \rangle$ directions suggests that the tweed microstructure is the result of $\langle 110 \rangle$ modulations of the lattice. Furthermore, the short length of the streaks in the FFT indicates a long wavelength modulation in real space. The lattice configuration responsible for the FFT of Fig. 6(d) is shown in Fig. 9 with its corresponding strain map. Looking down the $\langle 110 \rangle$ directions, long-wavelength $\langle 110 \rangle$ modulations can be seen. Taking the reciprocal of the length of the cross streaking yields a deformation tweed wavelength of approximately 50 to 70 Å. A simulation under the same conditions but for a lattice of 8×8 unit cells did not yield the tweed microstructure. This is consistent with the above observed tweed wavelength which is greater than the sample size 8×8 lattice.

These simulation results indicate that the tweed microstructure results from long-wavelength $\langle 110 \rangle$ displacement modulations of the basal plane (especially the oxygen-vacancy sublattice). It appears to occur as a result of strain accompanying the orthorhombic to tetragonal phase transition in *single domain* lattices which are fully oxygenated and perfectly ordered. Our findings here agree with the experimental work of Zhu, Suenaga, and Moodenbaugh³⁹ on the nature of the tweed texture in this system. This explanation of the tweed texture is also

consistent with those in classic studies of binary alloy systems undergoing a phase transformation involving a considerable elastic strain (see, for example, Ref. 77), in which the origin of the tweed texture is a static strain wave of displacement wave locked into the crystalline lattice. This is precisely the model we invoke for the tweed texture in the $\text{YBa}_2\text{Cu}_3\text{O}_z$ system under study, and the model for its formation is consistent with that proposed by Krumhansl in a recent overview of fine mesostructures in superconducting and other materials.⁷⁸ It is now also clear why other theories⁴⁹⁻⁵⁵ find unambiguous evidence for tweed, even though they treat the oxygen-vacancy variables in a simplified manner.

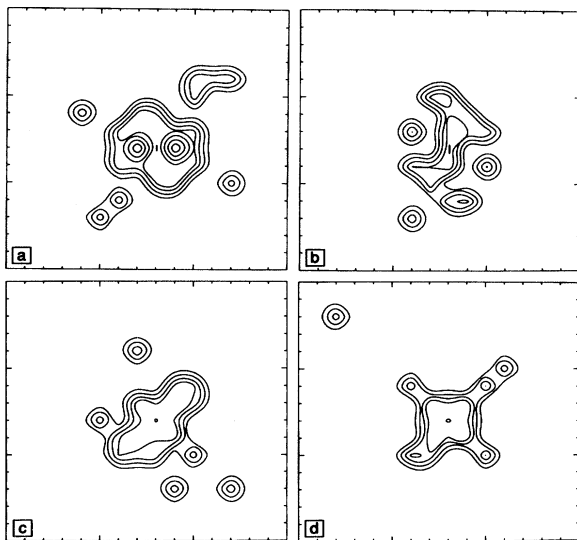


FIG. 8. (a)-(d) Contour plots of the (300) spots from the FFT's in Figs. 6(a)-6(d) respectively. (d) further highlights the $\langle 110 \rangle$ cross streaking which indicates the presence of the tweed microstructure.

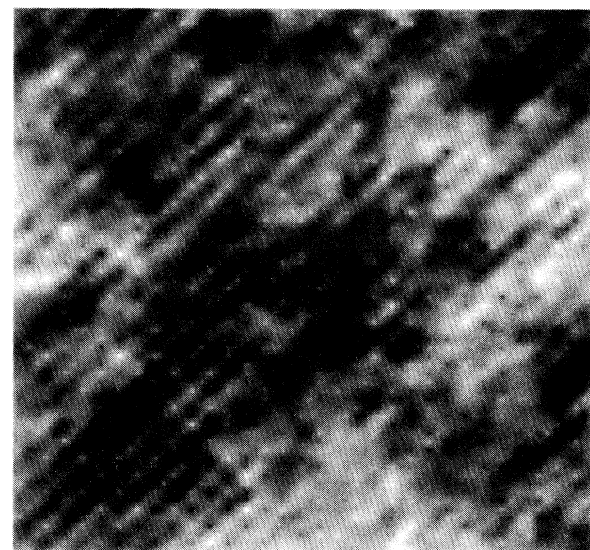
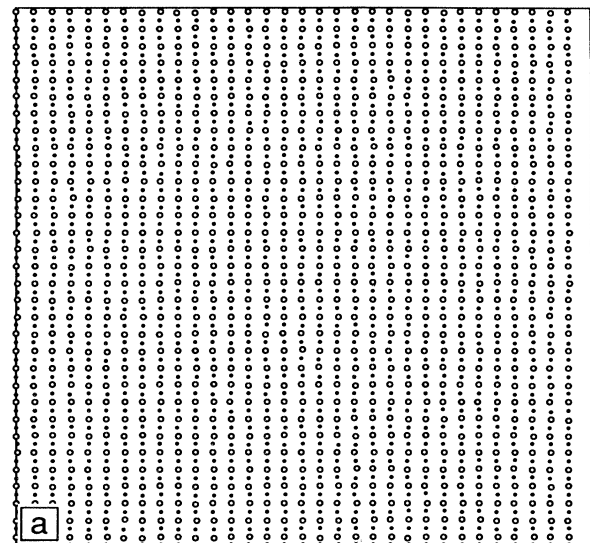


FIG. 9. (a) A photograph of the lattice whose FFT is shown in Fig. 6(d). (b) Strain map corresponding to the photograph of (a). Long-wavelength $\langle 110 \rangle$ modulations which give rise to the tweed microstructure can be seen.

D. Twinned domain formation and evolution

It has been shown in the previous two sections that the order-disorder, orthorhombic-tetragonal phase transition in $\text{YBa}_2\text{Cu}_3\text{O}_z$ is accompanied by strain which gives rise to various types of superstructures and tweed. Strain is induced in the system either as a consequence of the change in lattice parameter in the orthorhombic-tetragonal transformation or by a change in the system variables (temperature or chemical potential) in the orthorhombic phases. Many of the phenomena observed in this system (superstructures, tweed, twinning, etc.) are generally thought to arise as a direct result of this strain. Other theoretical treatments of elastic behavior⁴⁹⁻⁵⁵ have produced evidence for this effect.

Clearly, it is of interest to investigate how the system responds to the additional strain energy incurred during the orthorhombic-tetragonal phase transition. To best investigate the system's reactions it is useful to induce strain via rapid changes of temperature such as quenching or by the simple imposition of static isotropic strains. Rapid changes of temperature impose a thermal stress in addition to the one that occurs during the phase transition and it was therefore chosen as the method of inducing strain in the present study (so that the system response to large initial stresses could be observed).

To investigate the effect of strain on domain boundary formation and growth, a 64×64 unit-cell sample was disordered at 2640 K, then quenched to 330 K at a chemical potential of 0.0 J, and subsequently annealed.¹¹ This quenching run was performed seven times with the same starting configuration (disordered, fully oxygenated tetragonal material) so as to obtain an average of the kinetic processes involved (through the use of different random number seeds in the Monte Carlo simulation). It was found that all samples rapidly formed orthogonal *OI* domains upon quenching (see Fig. 10), so that while the lattice was microscopically orthorhombic, it was macroscopically tetragonal. As the system ordered, distinct orthorhombic domains formed. Domain boundaries were composed of $\langle 110 \rangle$ and/or $\langle 100 \rangle$ twins. By comparison to earlier simulation work⁷⁹ employing a static lattice approach (neglecting elasticity), the boundaries observed in this simulation are straight and coherent over long distances, much longer than the explicit second-nearest-neighbor distance of the spring constants included to model the effect of elasticity. Thus, the cooperative effect of the short-range force constants used in this model is to create a true elastic medium with effectively long-ranged interactions. However, nonphysical steps are occasionally observed along the domain boundaries [see Figs. 10(b) and 10(c)] that are not observed in experimental investigations. It is felt that if more displacive steps were taken for each diffusional step in the simulation, thus allowing a complete lattice relaxation after each oxygen-vacancy lattice rearrangement as discussed above, then even longer-range coherent domain boundaries would form, as is observed experimentally. Inspection of Fig. 10 reveals that as ordered domains come into contact with one another, coarsening proceeds via a competitive process in which the chains in some domains continue to increase at the

expense of those in others. This competition is concentrated at step defects and domain facet edges. Competitive coarsening leads to a smaller and smaller number of large *OI* domains and finally to one single *OI* lattice. The domain growth and evolution is accompanied by a macroscopic transformation from a tetragonal to an orthorhombic symmetry. This large-scale phase transformation can most easily be seen in Fig. 3 of Ref. 11 which shows a plot of the average basal plane lattice constants versus time averaged over the seven simulation runs. It was found that all samples attained complete orthorhombic order by at most 2800 MCSP. The lattice parameters for all samples were equal although the directions of the *a* and *b* axes varied in the final ordered configuration.

The two types of twin boundaries observed during domain formation ($\langle 110 \rangle$ and $\langle 100 \rangle$) display distinctive facet morphology in terms of copper-oxygen coordination. While the average oxygen coordination for the

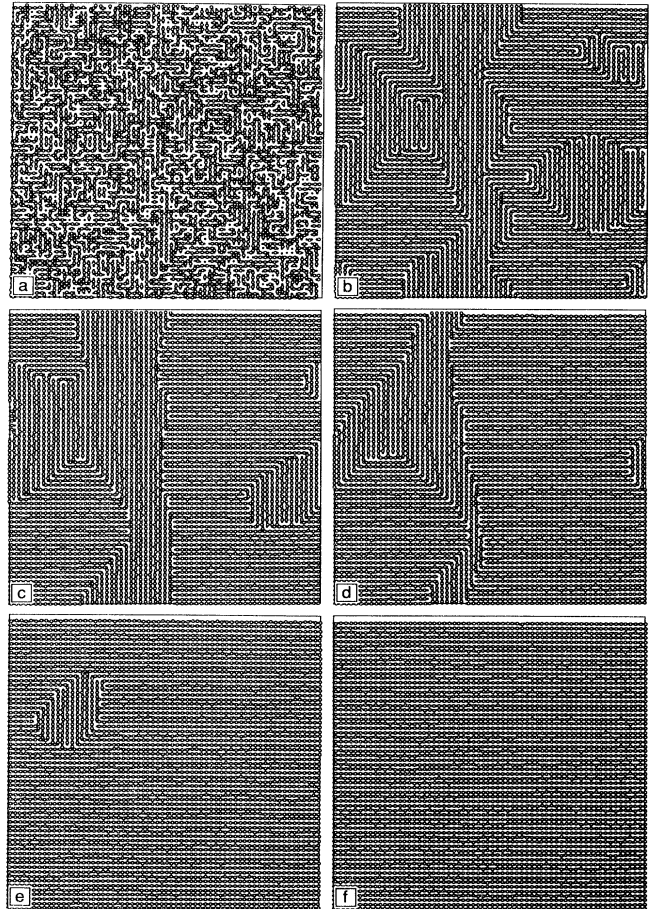


FIG. 10. Photographs of a 64×64 unit-cell lattice obtained by quenching a disordered tetragonal lattice at 2640 to 330 K at a chemical potential of 0.0J and annealing for (a) 0 MCSP, (b) 300 MCSP, (c) 800 MCSP, (d) 1800 MCSP, (e) 2300 MCSP, and (f) 2800 MCSP. The side of the square border is equal to 246 Å. Domains with twinned boundaries can be seen to form and then anneal out.

copper atoms at each boundary is four, the $\langle 110 \rangle$ type boundary consists solely of fourfold coordinated ions, whereas the $\langle 100 \rangle$ type boundary contains an approximately equal number of both threefold and fivefold coordinated copper ions leading to an average coordination of four as is expected for a stoichiometry of $z = 7.0$.

The above response to quenching (in terms of domain formation and coarsening) in $\text{YBa}_2\text{Cu}_3\text{O}_z$ is similar to that reported by Burmester and Wille,⁷⁹ who studied the system with the ASYNNNI model without elasticity. They observed that upon quenching short copper-oxygen chains rapidly nucleate throughout the basal plane (due to the attractive V_2 interaction) and continue to lengthen while preventing adjacent chains from forming (through V_1 and V_3). As orthogonal chains come into contact with one another, some chains continue to increase at the expense of others, leading to a smaller and smaller number of large OI domains and finally to one single OI domain. The authors further note that in the real material the domains are regularly organized and separated by twin boundaries and that although they observe very short $\{110\}$ domain walls, elasticity must be included to obtain the twin boundaries observed experimentally.

In the present simulation the lattice thus underwent the reverse of an orthorhombic-tetragonal, order-disorder phase transition. A strain accompanies this transition (as evidenced by the change in lattice parameters discussed above) and the lattice responds to this strain as well as the strain incurred during quenching (due to thermal expansion) by forming domains with twinned boundaries. The study of twinning in $\text{YBa}_2\text{Cu}_3\text{O}_z$ is well developed and while it has been found that with no constraints during the phase transformation, the lattice is free to relax and thus no twinning occurs,⁸⁰ it has also been determined that $\text{YBa}_2\text{Cu}_3\text{O}_z$ forms $\langle 110 \rangle$ twins⁴²⁻⁴⁸ in the orthorhombic phase upon undergoing the orthorhombic-tetragonal phase transition while under the influence of additional stresses (constraints such as from other grains in a polycrystalline sample, etc.). These twins occur as a way to minimize the free energy resulting from the strain produced by the orthorhombic deformation. During the phase transition, the $\{110\}$ mirror planes are the symmetry elements lost in going from the tetragonal ($4/mmm$) to the OI (mmm) phase and thus act as preferential planes for coherent twin formation (they are strain free during the transformation). In the current study, the constraint on the system caused by quenching results in the formation of twins. Although the sample size in this study is not large enough to form the type of twin bands ($\approx 500 \text{ \AA}$) observed,⁴⁸ the twinned domain boundaries in this simulation indicate a similar response as a way to alleviate the strain in the system.

Immediately after quenching the disordered tetragonal microstructure is observed to have average lattice parameters of $a_0 = b_0 \approx 3.84 \text{ \AA}$ while the completely ordered orthorhombic structure (OI) after 2800 MCSP has attained average lattice parameters of $a_0 = 3.8080 \text{ \AA}$ and $b_0 = 3.8846 \text{ \AA}$. This is to be compared to the experimentally measured lattice constants at 300 K, which for the $z = 7.0$ phase are $a_0 = 3.8206 \text{ \AA}$ and $b_0 = 3.8851 \text{ \AA}$ as found by profile refinement of high-resolution neutron

powder data.⁸¹ Thus the simulated sample has smaller lattice constants than those measured experimentally, although the difference is relatively small. It is most likely that this discrepancy is due to the considerable residual strain that is still present in the material (see Fig. 11 and discussion below). A continuation of the annealing process for longer times was found to lead to further macroscopic expansion of the lattice. Also to be noted in Fig. 3 of Ref. 11 is the staircase dependence of the temporal behavior of the lattice constants during annealing. This phenomenon is a consequence of the relatively small size of the simulation sample which leads to exaggerated abrupt changes in the average lattice parameter each time a domain is completely removed through annealing. It also indicates that deformations propagate very rapidly throughout the simulation lattice. Furthermore, one can observe in Fig. 3 of Ref. 11 the relatively smooth variation of the b_0 lattice parameter, but with large statistical scatter, in stark contrast to the uniform but staircase variation of the a_0 lattice parameter. This is a consequence of the presence of the oxygen atoms which mediate the copper-copper bond along the b_0 direction. These atoms will tend to smooth out strain response along this

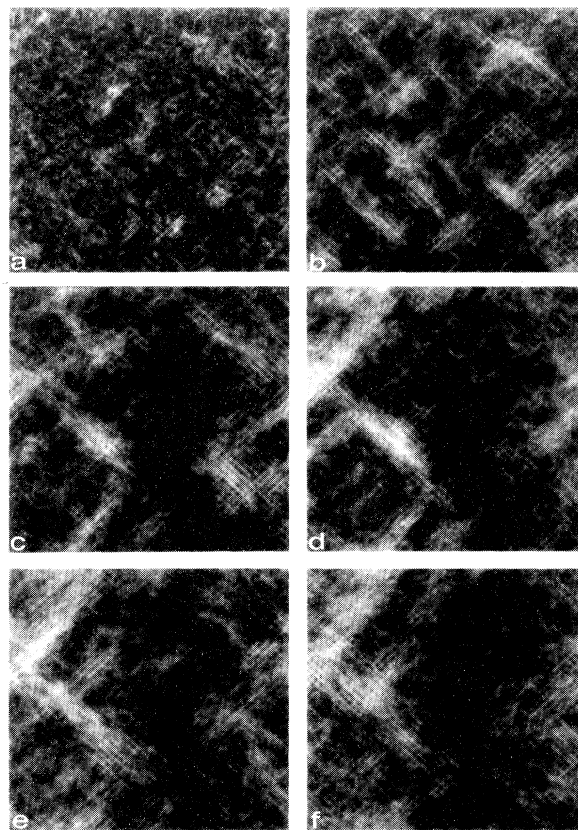


FIG. 11. Strain plots of the photographs in Fig. 10 in which white represents the regions of maximum strain and black represents the areas of minimum strain. The areas of highest strain can be seen at the domain boundaries. Each plot is $246 \text{ \AA} \times 246 \text{ \AA}$.

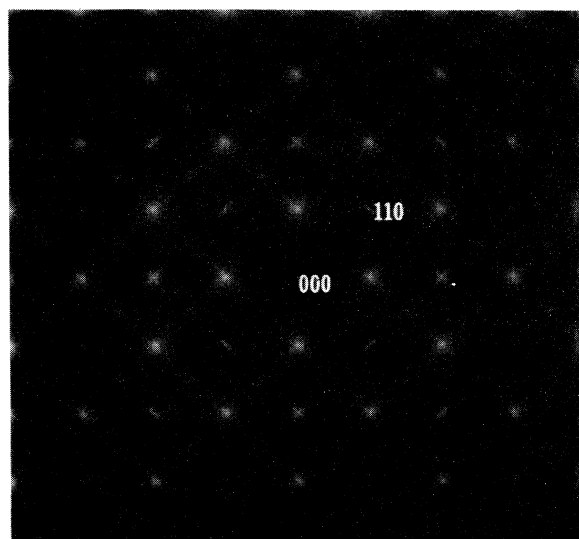


FIG. 12. FFT of the snapshot in Fig. 10(f). Superlattice spots indicative of the $\sqrt{2}a_0 \times \sqrt{2}a_0$ structure can be seen.

direction as compared to the a_0 direction where there are no intermediate atoms, leading to the observed behavior.

To further investigate the effects due to elasticity, strain plots were again examined. Figure 11 shows the strain plots corresponding to the basal plane configurations of Fig. 10. Strain can clearly be seen at the domain boundaries, especially the $\{110\}$ twin boundaries. As the domains anneal out some residual strain remains. However, more and more strain associated with the $\sqrt{2}a_0 \times \sqrt{2}a_0$ structure can be seen. Corresponding FFT intensities (Fig. 12) reveal that the $\sqrt{2}a_0 \times \sqrt{2}a_0$ structure does indeed appear. Note also the streaking about the spots in the $[110]$ or $[1\bar{1}0]$ depending on the quadrant of the FFT. This streaking is believed to arise from continuous displacements normal to the two sets of orthogonal $\{110\}$ planes: the (110) and the $(1\bar{1}0)$, respectively. The fact that the displacements are continuous results in a streak rather than two distinct, close spots which would be observed for a discrete displacement of $\{110\}$ planes in a normal direction.

Thus, the response to a large stress on the initially constrained basal plane of $\text{YBa}_2\text{Cu}_3\text{O}_z$ is to form domains. These domains alleviate the stress by forming twinned boundaries. As the lattice anneals and becomes less constrained, these twinned domains anneal out leaving some residual strain which causes the $\sqrt{2}a_0 \times \sqrt{2}a_0$ structure to form as discussed in a previous section.

IV. CONCLUSIONS

A computer simulation technique for modeling phenomena due to elasticity associated with order-disorder phase transformations is presented. The method currently uses the strict harmonic approximation as well as the grand canonical stress ensemble and employs the Monte Carlo technique. The model was applied to study the

effects of the strain that accompanies the order-disorder, orthorhombic-tetragonal phase transformation in the basal plane of $\text{YBa}_2\text{Cu}_3\text{O}_z$. Both phenomena due to oxygen ordering which have previously been observed with static models as well as phenomena due to the effects of strain were observed. Deformation superstructures, tweed, and domains with coherent twinned domain boundaries were seen to form as a result of strain in the system. The $\sqrt{2}a_0 \times \sqrt{2}a_0$ superstructure was found to arise and its formation attributed to strain dissipation in the ordered OI material via a softened mode with wave vector $\mathbf{q} = [\frac{1}{2} \frac{1}{2} 0]$ acting on the oxygen-vacancy sublattice in the basal plane of the material. The tweed microstructure was found to occur as a result of long-wavelength $\langle 110 \rangle$ phonons. Upon ordering, the system forms domains which organize themselves into twins and coherent boundaries so as to minimize resulting strain energy.

In view of the rich variety of elastic effects that can be studied with the present approach, it would be very interesting to apply this method to other situations involving the Y-Ba-Cu-O system that have been studied with static lattice models. Notably, the effects of dopants substituting for Cu in the basal plane are accompanied by large stresses and lead to displaced atomic positions that do not coincide with those of the Cu-O parent lattice.⁸²⁻⁸⁵ Extensions of the ASYNNNI model to incorporate cation doping on the Cu sites have been proposed,^{82,84} but do not include elasticity and are therefore restricted in predictive power. The Semenovskaya and Khachatryan approach⁴⁹⁻⁵¹ has been applied to this problem⁸⁵ with very interesting results, particularly a striking agreement with experimentally observed tweed patterns. Another issue of interest is the response of the $\text{YBa}_2\text{Cu}_3\text{O}_z$ system to external stresses, such as those used to mechanically detwin the material. A static model based on the ASYNNNI Hamiltonian has recently been developed to investigate the nature of the detwinning process⁸⁶ and could benefit from a full treatment of the elasticity in the system. Since the present work shows the richness of the systems response to internal stresses, it would be particularly useful to investigate the effects of macroscopic strains. To study some of these further issues and as a natural extension of the current study, it would also be very useful to include the elastic degrees of freedom of the remainder of the structure. Generalizations of the ASYNNNI model including EPI's between basal plane oxygen sites and the apical oxygen sites have been proposed⁸⁷ and could form the starting point of a more general, three-dimensional oxygen-ordering model including elasticity.

As was mentioned at the outset, the proposed methodology is not restricted to $\text{YBa}_2\text{Cu}_3\text{O}_z$. An application that comes immediately to mind would be the study of martensitic transformations.⁵⁶ Note that for the construction of an appropriate Hamiltonian one is not required to use spring constants, i.e., to rely on the harmonic approximation, but rather one could use instead an appropriate potential, as may be obtained by any one of a range of techniques (embedded atom method, effective medium theories, etc.). In the case of long-range elastic potentials

the evaluation of the change in energy, ΔH , necessary at each Monte Carlo step may become cumbersome and one may also have to perform an Ewald summation to eliminate boundary effects. For $\text{YBa}_2\text{Cu}_3\text{O}_z$ interaction potentials have been developed by Baetzold⁸⁸ and by Wright and Butler,⁸⁹ but the present work shows that the harmonic approximation is sufficient to understand the vast majority of strain-related phenomena in this system. The same may very well be true in alloys undergoing martensitic transformations. It is also worth mentioning that the proposed methodology is well suited for implementation on massively parallel computers. The Monte Carlo simulation for the static ASYNNTI model has been ported to such computers⁹⁰ and work is currently underway to extend this code to include the elastic terms introduced here. The same considerations to accomplish correct and efficient parallelization discussed elsewhere⁹⁰ continue to hold. For longer-range potentials one can employ techniques from parallel molecular dynamics⁹¹ to parallelize the computer codes. Clearly, this kind of parallel machine will allow quite large systems (comparable in size to actual grains in the material) to be studied over long time periods and will likely open up the way to new insights and an unprecedented level of realistic behavior with regard to the sizes and time scales of the simulations.

Although the present simulation has given a very satisfactory description of elastic effects in $\text{YBa}_2\text{Cu}_3\text{O}_z$, a number of questions still remain, such as the nature of the transition lines in the phase diagram and the possibility of other $\sqrt{2}$ based structures associated with devil's staircase phases or at other compositions. These issues are currently under study. With regard to the underlying framework, it would be very satisfactory to derive the EPI's and spring constants from a single set of first-principles electronic structure calculations, but it remains to be seen how this can be accomplished. At a more fundamental level the kinetics of the phase transitions in strain-coupled systems is expected to be different from nucleation-and-growth kinetics, as demonstrated by Marais *et al.*⁹² for a simplified model. It would be very interesting to establish this same type of behavior for a more realistic Hamiltonian.

ACKNOWLEDGMENTS

This work was supported by the Director, Office of Energy Research, Office of Basic Energy Sciences, Materials Sciences Division of the U.S. Department of Energy under Contract No. DE-AC03-76SF00098. M.G. would like to thank the Office of Naval Research for financial support.

- ¹J. S. Faulkner and R. G. Jordan, *Metallic Alloys: Experimental and Theoretical Perspectives* (Kluwer, Dordrecht, 1994), and references therein.
- ²C. Itzykson and J. M. Drouffe, *Statistical Field Theory* (Cambridge University Press, Cambridge, 1989).
- ³R. Kikuchi, *Phys. Rev.* **81**, 988 (1951).
- ⁴D. de Fontaine, *Solid State Phys.* **34**, 73 (1979).
- ⁵K. Binder, *Monte Carlo Methods in Statistical Physics* (Springer, Berlin, 1979); *Applications of the Monte Carlo Method in Statistical Physics* (Springer, Berlin, 1984).
- ⁶O. G. Mouritsen, *Computer Studies of Phase Transitions and Critical Phenomena* (Springer, Berlin, 1984).
- ⁷V. Privman, *Finite Size Scaling and Numerical Simulation of Statistical Systems* (World Scientific, Singapore, 1990).
- ⁸W. G. Hoover, *Molecular Dynamics* (Springer, Berlin, 1986).
- ⁹G. Ciccotti, D. Frenkel, and I. R. McDonald, *Simulation of Liquids and Solid* (North-Holland, Amsterdam, 1987).
- ¹⁰M. Goldman, C. P. Burmester, L. T. Wille, and R. Gronsky, *Phys. Rev. B* **50**, 1337 (1994).
- ¹¹M. Goldman, C. P. Burmester, L. T. Wille, and R. Gronsky, *Philos. Mag. Lett.* **70**, 65 (1994).
- ¹²R. Beyers and T. M. Shaw, *Solid State Phys.* **42**, 135 (1989).
- ¹³J. L. Moran-Lopez and I. K. Schuller, *Oxygen Disorder Effects in High- T_c Superconductors* (Plenum, New York, 1990).
- ¹⁴D. de Fontaine, G. Ceder, and M. Asta, *Nature* **343**, 544 (1990).
- ¹⁵A. A. Aligia, *Europhys. Lett.* **18**, 181 (1992).
- ¹⁶D. Adelman, C. P. Burmester, L. T. Wille, P. A. Sterne, and R. Gronsky, *J. Phys. Condens. Matter* **4**, L585 (1992).
- ¹⁷L. T. Wille, A. Berera, and D. de Fontaine, *Phys. Rev. Lett.* **60**, 1065 (1988).
- ¹⁸R. Kikuchi and J. S. Choi, *Physica C* **160**, 347 (1989).
- ¹⁹N. C. Bartelt, T. L. Einstein, and L. T. Wille, *Phys. Rev. B* **40**, 10759 (1989).
- ²⁰P. A. Sterne and L. T. Wille, *Physica C* **162-164**, 223 (1989).
- ²¹G. Ceder, M. Asta, W. C. Carter, M. Kraitchman, D. de Fontaine, M. E. Mann, and M. Sluiter, *Phys. Rev. B* **41**, 8698 (1990).
- ²²T. Aukrust, M. A. Novotny, P. A. Rikvold, and D. P. Landau, *Phys. Rev. B* **41**, 8772 (1990).
- ²³P. A. Sterne and L. T. Wille, in *Atomic Scale Calculations of Structure in Materials*, edited by M. S. Daw and M. A. Schluter, MRS Symposia Proceedings No. 193 (Materials Research Society, Pittsburgh, 1990), p. 35.
- ²⁴V. E. Zubkus, E. E. Tornau, S. Lapinskas, and P. J. Kundrotas, *Phys. Rev. B* **43**, 13112 (1991).
- ²⁵D. K. Hilton, B. M. Gorman, P. A. Rikvold, and M. A. Novotny, *Phys. Rev. B* **46**, 381 (1992).
- ²⁶J. Oitmaa, Y. Jie, and L. T. Wille, *J. Phys. Condens. Matter* **5**, 4161 (1993).
- ²⁷W. Selke and G. V. Uimin, *Physica C* **214**, 37 (1993).
- ²⁸A. Santoro, S. Miraglia, F. Beech, S. A. Sunshine, D. W. Murphy, L. F. Schneemeyer, and J. V. Waszczak, *Mater. Res. Bull.* **22**, 1007 (1987).
- ²⁹R. J. Cava, A. W. Hewat, E. A. Hewat, B. Batlogg, M. Marezio, K. M. Rabe, J. J. Krajewski, W. F. Peck, Jr., and L. W. Rupp, Jr., *Physica C* **165**, 419 (1990).
- ³⁰K. B. Blagoev and L. T. Wille, *Phys. Rev. B* **48**, 6588 (1993).
- ³¹Note that since Ref. 30 was submitted further experimental evidence for coexistence has been obtained: M. Iliev, C. Thomsen, V. Hadjiev, and M. Cardona, *Phys. Rev. B* **47**, 12341 (1993); H. Lutgemeier, I. Heinmaa, and A. V. Egorov, *Phys. Scr.* **T49**, 137 (1993).
- ³²D. J. Werder, C. H. Chen, and G. P. Espinosa, *Physica C* **173**,

- 285 (1991).
- ³³T. Krekels, T. S. Shi, J. Reyes-Gasga, G. Van Tendeloo, J. Van Landuyt, and S. Amelinckx, *Physica C* **167**, 677 (1990).
- ³⁴C. H. Chen, D. J. Werder, L. F. Schneemeyer, P. K. Gallagher, and J. V. Waszczak, *Phys. Rev. B* **38**, 2888 (1988).
- ³⁵Th. Zeiske, D. Hohlwein, R. Sonntag, F. Kubanck, and G. Collin, *Z. Phys. B* **86**, 11 (1992).
- ³⁶R. Sonntag, D. Hohlwein, T. Brückel, and G. Collin, *Phys. Rev. Lett.* **66**, 1497 (1991).
- ³⁷W. Schwarz, O. Blaschko, G. Collin, and F. Marucco, *Phys. Rev. B* **48**, 6513 (1993).
- ³⁸Y. Zhu, M. Suenaga, and A. R. Moodenbaugh, *Philos. Mag. Lett.* **62**, 51 (1990).
- ³⁹Y. Zhu, M. Suenaga, and A. R. Moodenbaugh, *Ultramicroscopy* **37**, 341 (1991).
- ⁴⁰Y. Zhu, M. Suenaga, and J. Taftø, *Philos. Mag. Lett.* **64**, 29 (1991).
- ⁴¹G. Lacayo and G. Kästner, *Phys. Status Solidi A* **131**, K7 (1992).
- ⁴²E. A. Hewat, M. Dupuy, A. Bourret, J. J. Capponi, and M. Marezio, *Solid State Commun.* **64**, 517 (1987).
- ⁴³M. Hervieu, B. Domenges, C. Michel, G. Heger, J. Provost, and B. Raveau, *Phys. Rev. B* **36**, 3920 (1987).
- ⁴⁴Y. Syono, M. Kikuchi, K. Oh-Ishi, K. Hiraga, H. Arai, Y. Matsui, N. Kobayashi, T. Sasaoka, and Y. Muto, *Jpn. J. Appl. Phys.* **26**, 498 (1987).
- ⁴⁵H. W. Zandbergen, G. Van Tendeloo, T. Okabe, and S. Amelinckx, *Phys. Status Solidi A* **103**, 45 (1987).
- ⁴⁶A. F. Moodie and H. J. Whitfield, *Ultramicroscopy* **24**, 329 (1988).
- ⁴⁷J. F. Smith and D. Wohlleben, *Z. Phys. B* **72**, 323 (1988).
- ⁴⁸G. Van Tendeloo and S. Amelinckx, *J. Electron Microsc. Tech.* **8**, 285 (1988).
- ⁴⁹S. Semenovskaya and A. G. Khachatryan, *Phys. Rev. Lett.* **67**, 2223 (1991).
- ⁵⁰S. Semenovskaya and A. G. Khachatryan, *Phys. Rev. B* **46**, 6511 (1992).
- ⁵¹S. Semenovskaya and A. G. Khachatryan, *Philos. Mag. Lett.* **66**, 105 (1992).
- ⁵²E. Salje and K. Parlinski, *Supercond. Sci. Technol.* **4**, 93 (1991).
- ⁵³K. Parlinski, V. Heine, and E. K. H. Salje, *J. Phys. Condens. Matter* **5**, 497 (1993).
- ⁵⁴K. Parlinski, E. K. H. Salje, and V. Heine, *Acta Metall. Mater.* **41**, 839 (1993).
- ⁵⁵K. Parlinski and M. Sternik, *J. Phys. Condens. Matter* **6**, 237 (1994).
- ⁵⁶G. B. Olson and W. S. Owen, *Martensite* (ASM International, Materials Park, OH, 1992).
- ⁵⁷D. de Fontaine, L. T. Wille, and S. C. Moss, *Phys. Rev. B* **36**, 5709 (1987).
- ⁵⁸N. Pyka, W. Reichardt, L. Pintschovius, S. L. Chaplot, P. Schweiss, A. Erb, and G. Müller-Vogt, *Phys. Rev. B* **48**, 7746 (1993).
- ⁵⁹P. Schweiss, W. Reichardt, M. Braden, G. Collin, G. Heger, H. Claus, and A. Erb, *Phys. Rev. B* **49**, 1387 (1994).
- ⁶⁰C. Ramakrishnan and N. Krishnamurthy, *Solid State Commun.* **79**, 363 (1991).
- ⁶¹J. H. Weiner, *Statistical Mechanics of Elasticity* (Wiley, New York, 1983).
- ⁶²B. K. Chakrabarti, N. Battacharyya, and S. K. Sinha, *J. Phys. C* **15**, L777 (1982).
- ⁶³A. F. S. Moreira and W. Figueiredo, *Phys. Rev. B* **46**, 2891 (1992).
- ⁶⁴A. Aharony and A. D. Bruce, *Phys. Rev. Lett.* **33**, 427 (1974); **42**, 462 (1979).
- ⁶⁵R. Kirkuchi and A. Beldjenna, *Physica A* **182**, 617 (1992).
- ⁶⁶A. Finel, *Prog. Theor. Phys. Suppl.* **115**, 59 (1994).
- ⁶⁷M. Parrinello and A. Rahman, *Phys. Rev. Lett.* **45**, 1196 (1980).
- ⁶⁸L. T. Wille and D. de Fontaine, *Phys. Rev. B* **37**, 2227 (1988).
- ⁶⁹J. Stolze, *Phys. Rev. Lett.* **64**, 970 (1990).
- ⁷⁰C. C. A. Günther, P. A. Rikvold, and M. A. Novotny, *Phys. Rev. B* **42**, 10738 (1990).
- ⁷¹A. A. Aligia, J. Garcés, and H. Bonadeo, *Phys. Rev. B* **42**, 10226 (1990).
- ⁷²M. A. Alario-Franco, C. Chaillout, J. J. Capponi, J. Chénavas, and M. Marezio, *Physica C* **156**, 455 (1988).
- ⁷³D. de Fontaine, M. Asta, G. Ceder, R. McCormack, and G. van Tendeloo, *Europhys. Lett.* **19**, 229 (1992).
- ⁷⁴A. A. Aligia, *Europhys. Lett.* **26**, 153 (1994).
- ⁷⁵D. de Fontaine, *Europhys. Lett.* **26**, 155 (1994).
- ⁷⁶P. A. Stene and L. T. Wille (unpublished).
- ⁷⁷L. E. Tanner, A. R. Pelton, and R. Gronsky, *J. Phys. (Paris) Colloq.* **43** C4, 12 (1982).
- ⁷⁸J. A. Krumhansl, in *Lattice Effects in High T_c Superconductors*, edited by Y. Bar-Yam, T. Egami, J. Mustre de-Leon, and A. R. Bishop (World Scientific, Singapore, 1992).
- ⁷⁹C. P. Burmester and L. T. Wille, *Phys. Rev. B* **40**, 8795 (1989).
- ⁸⁰C. Thomsen, M. Cardona, R. Liu, B. Gegenheimer, and A. Simon, *Physica C* **153-155**, 1756 (1988).
- ⁸¹J. J. Capponi, C. Chaillout, A. W. Hewat, P. Lejay, M. Marezio, N. Nguyen, B. Raveau, J. L. Soubeyrou, J. L. Tholence, and R. Tournier, *Europhys. Lett.* **3**, 1301 (1987).
- ⁸²C. P. Burmester, L. T. Wille, and R. Gronsky, *Solid State Commun.* **77**, 693 (1991).
- ⁸³X. Jiang, P. Wochner, S. C. Moss, and P. Zschack, *Phys. Rev. Lett.* **67**, 2167 (1991).
- ⁸⁴Z. X. Cai, Y. Zhu, and D. O. Welch, *Phys. Rev. B* **46**, 11014 (1992).
- ⁸⁵S. Semenovskaya, Y. Zhu, M. Suenaga, and A. G. Khachatryan, *Phys. Rev. B* **47**, 12182 (1993).
- ⁸⁶C. P. Burmester, L. T. Wille, and R. Gronsky, *Physica C* **230**, 16 (1994).
- ⁸⁷J. M. Sanchez and J. L. Moran-Lopez, *Solid State Commun.* **79**, 151 (1991).
- ⁸⁸R. C. Baetzold, *Phys. Rev. B* **38**, 11304 (1988).
- ⁸⁹N. F. Wright and W. H. Butler, *Phys. Rev. B* **42**, 4219 (1990).
- ⁹⁰L. T. Wille, J. L. Rogers, C. P. Burmester, and R. Gronsky, *Future Generation Comp. Syst.* **10**, 331 (1994).
- ⁹¹K. M. Nelson, C. F. Cornwell, and L. T. Wille, *Comput. Mater. Sci.* **2**, 525 (1994).
- ⁹²S. Marais, V. Heine, C. Nex, and E. Salje, *Phys. Rev. Lett.* **66**, 2480 (1991).

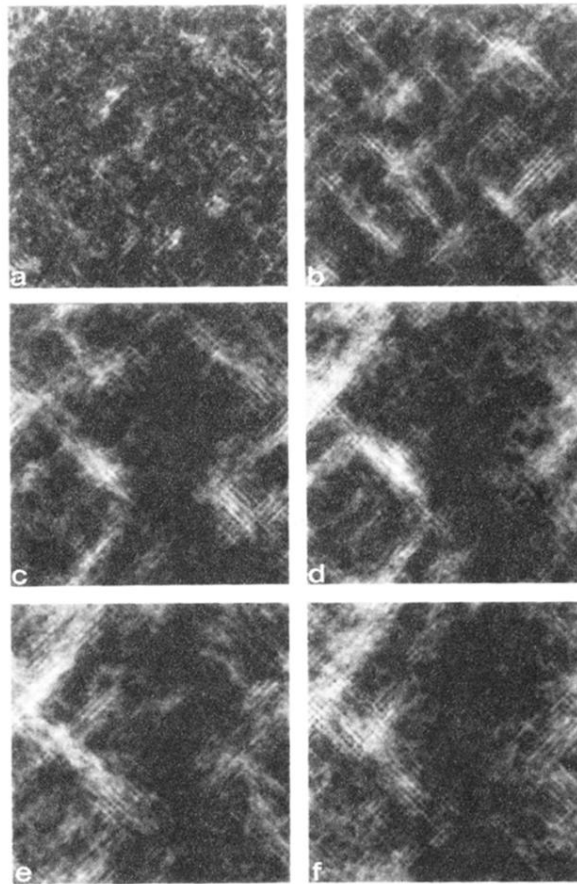


FIG. 11. Strain plots of the photographs in Fig. 10 in which white represents the regions of maximum strain and black represents the areas of minimum strain. The areas of highest strain can be seen at the domain boundaries. Each plot is $246 \text{ \AA} \times 246 \text{ \AA}$.

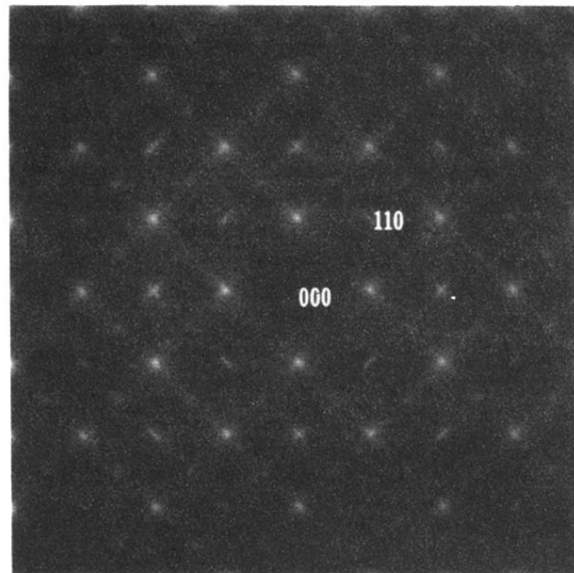


FIG. 12. FFT of the snapshot in Fig. 10(f). Superlattice spots indicative of the $\sqrt{2}a_0 \times \sqrt{2}a_0$ structure can be seen.

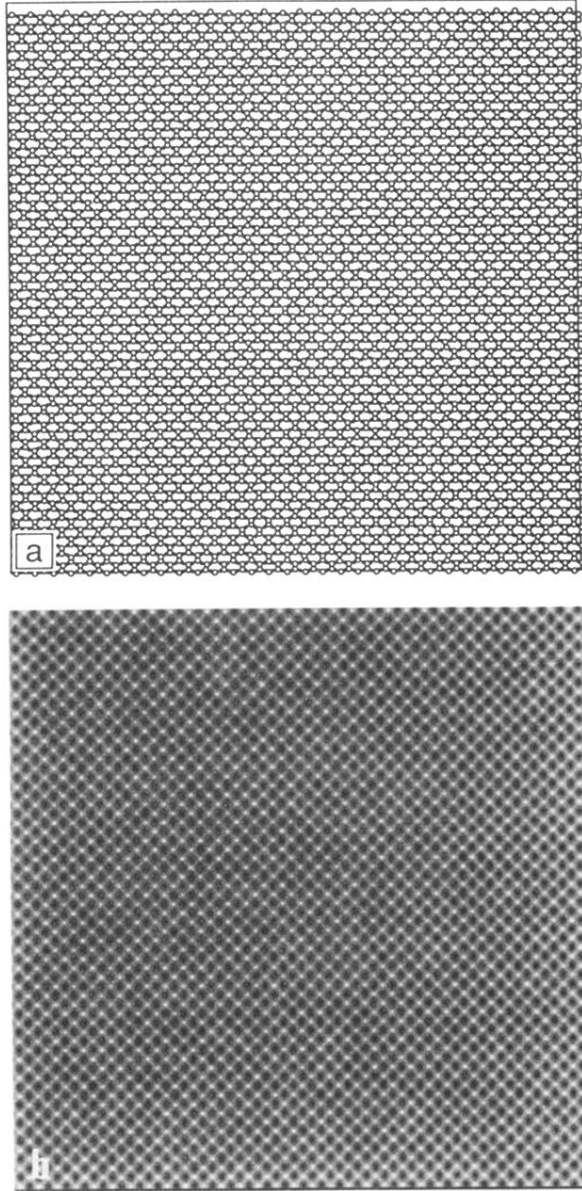


FIG. 5. Simulation of the $\sqrt{2}$ structure. (a) Idealized photograph of the $\sqrt{2}$ superstructure. (b) Simulated strain map of the $\sqrt{2}$ structure based on the photograph of (a).

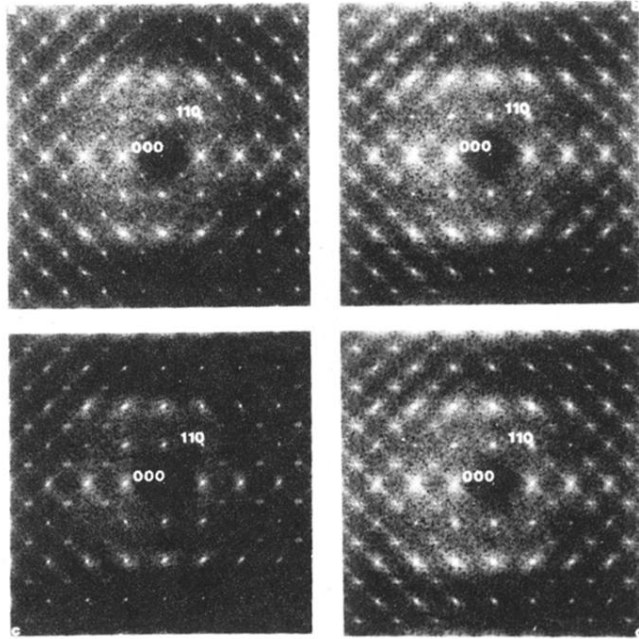


FIG. 6. A time sequence of FFT's obtained after annealing a 32×32 unit-cell artificially deformed tetragonal lattice at 660 K and a chemical potential of 0.0J for (a) 1000 MCSP, (b) 4000 MCSP, (c) 7000 MCSP, and (3) 10 000 MCSP. The $\sqrt{2}a_0 \times \sqrt{2}a_0$ superlattice reflections can be seen to appear diffusely (a), to sharpen (b), to disappear (c), and to reappear diffusely (d), indicating a cycling of the phase.

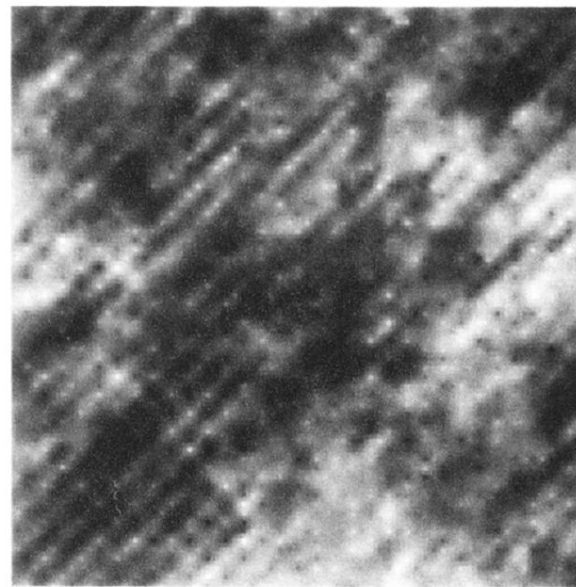
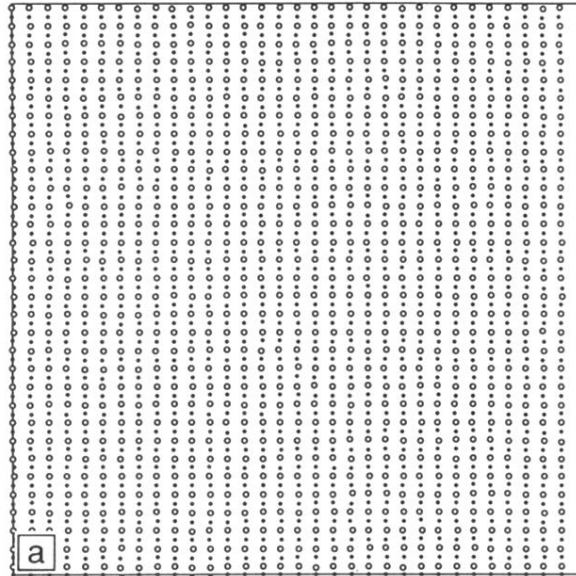


FIG. 9. (a) A photograph of the lattice whose FFT is shown in Fig. 6(d). (b) Strain map corresponding to the photograph of (a). Long-wavelength $\langle 110 \rangle$ modulations which give rise to the tweed microstructure can be seen.